Instrumentation Error Correction within Merging Units

A.P. Meliopoulos, *Fellow, IEEE*, George Cokkinides, *Member, IEEE*, Jiahao Xie and Yuan Kong
School of Electrical and Computer Engineering, Georgia Institute of Technology, Atlanta, GA, U.S.A.

***Abstract*—** As relays and merging units are becoming more sophisticated by using higher resolution (higher sampling rates) and advanced protection functions and applications, the errors from instrumentation channels remain practically the same. As a matter of fact, instrumentation channel errors are now much higher than the errors introduced by the data acquisition even in earlier generations of sensor-less systems. Efforts to account and correct for instrumentation channel errors date back several decades. This paper presents recent developments in instrumentation channel error correction. We present a dynamic state estimation method which uses detailed mathematical models of the entire instrumentation channel and dynamic state estimation to provide a correction for the instrumentation channel error on a sample by sample basis. We organize the method in such a way that the merging unit reports directly primary values that have been corrected for instrumentation error. We propose that this method be an integral part of merging units. The paper presents examples that indicate the effectiveness of the method to correct instrumentation channel errors including errors resulting from saturation of CTs.

***Index Terms*-- Merging Units, Instrumentation Channel Error, Dynamic State Estimation.**

INTRODUCTION

The performance of any protection system is always dependent upon the quality and validity of the measurements. This has been recognized for any protective system for years. The relay instrumentation subsystem provides the proper interface between the high current electric power system and the relays that operate at relatively low voltage and current. Ideally, the secondary voltage and current of instrumentation channels should be an exact scaled replica of the primary quantities. In practice, however, the instrumentation channel will introduce errors which are typically much higher than the errors introduced by the relay or merging unit analog input and A/D converters. In addition, during faults, there is the possibility of CT saturation which typically leads to distorted secondary current waveforms and associated large errors. In some cases, distorted measurements may result in mal-operation of protective relays [1]. Therefore, it is essential to come up with methods which can correct instrumentation channel errors.

Current instrumentation channels have received substantial attention due to the saturation of CTs. Much work has been devoted to research on compensating the CT's secondary current, which can be classified into three categories: (1) Compensating the secondary current via computation of the magnetizing current [2-4]. Reference [2] proposes estimation of the magnetizing current by calculating the flux of the current transformer, then adding the magnetizing current to the secondary current to achieve current compensation. This method can perform well, but it can only work under the condition that there is no remnant flux in the current transformer, which is not true during transients including fault condition. Also, this method only works well for a specific magnetization curve, which cannot be universally applied in practice. Another approach in reference [3-4] applies morphological lifting scheme to the detection of the first saturation point of the current transformer. Although this approach can avoid the effect of remnant flux, it relies too much on the precise detection of the first saturation point, which is greatly affected by disturbance and noise. More importantly, this method can not achieve on-line correction of CT primary current, which does not satisfy the real-time requirements of protective relays. (2) Reconstructing the secondary current using artificial neural network (ANN) [5-8]. The ANN is utilized to learn the nonlinear characteristics of magnetizing current and then to reconstruct the secondary current. However, there is much difficulty in choosing the appropriate ANN parameters to fit different CT types in practice. Again, this method does not achieve the on-line correction of CT primary current. (3) Estimating the secondary current utilizing the unsaturated waveform portions [9-12]. This method separates the secondary current into unsaturated part and saturated part based on setting an exact reference point (RP). Then, the extracted unsaturated portion will be used in the current estimation. However, it is not easy to accurately identify the RP and this method will fail to obtain a good estimation without an accurate RP. Reference [13] investigates an on-line method to correct the errors introduced by the instrument transformers steady -state waveform measurements. The repetitive learning control is used to track the transformer output waveforms. The work presented in this paper is focused on a voltage instrument transformer. Performance when the method is applied to a current transformer is not provided. While the objective of this method is to provide an online method, the required computations and training make is impractical for today's speed requirements.

The introduction of merging units enables error correction within the merging unit. Specifically, each instrumentation channel of a merging unit can be designed to provide corrected primary values. This paper addresses this goal and proposes an error correction method for the entire instrumentation channel using dynamic state estimation. The method is dependent upon a high fidelity model of the instrumentation channel. We propose to cast this model as a quadratized dynamic model of the entire instrumentation

channel. The dynamic state estimation uses this model. To simplify the analytics, the quadratized dynamic model is integrated using the quadratic integration method to generate the Algebraic Quadratic Companion Form (AQCF) of the instrumentation channel. The measurements expressed via the AQCF model providing a quadratic dynamic model of measurements [14]. The dynamic state estimation (DSE) is formulated using the quadratic measurement models. The dynamic state estimation operates on the sampled values. The computations are performed within the sampling period making the method real time. This method is an integral part of merging units so that that the merging unit reports directly estimated primary values which have been corrected.

This paper presents the method with emphasis on current instrumentation channels. It should be understood that the method is equally applicable to voltage instrumentation channels.

DYNAMIC MEASUREMENT MODEL OF CURRENT INSTRUMENTATION CHANNEL

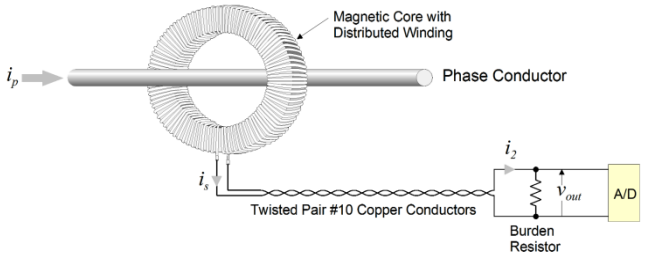

Figure 1: Typical current instrumentation channel configuration

A typical current instrumentation channel configuration is shown in Fig. 1. Three components can be identified: the current transformer, the instrumentation cable and the burden (resistor). The current instrumentation subsystem is used to convert the high current of the power system into instrumentation level currents that can be fed into the Merging Unit. Standard currents for Merging Unit are 5A and 1A. Ideally, the currents fed into the merging unit should be scaled replicas of the high currents of electric power system. Practically, however, the current instrumentation channels introduce errors that can distort the secondary waveforms when CT saturates. In some cases, these errors will even cause the mal-operation of the relay. Therefore, to make the protection scheme reliable, it is essential to correct the errors introduced by the current instrumentation channels.

The problem of current instrumentation channel error correction is stated as follows: a secondary measurement is taken at the merging unit (current through the burden). It is desirable to compute the primary current as accurate as possible. The computation is performed via a dynamic state estimation that provides the best estimate of the primary current. Subsequently, the merging unit streams the best estimate of the primary current upstream for utilization by the logical nodes of the protection and control system.

Dynamic Quadratized Measurement Model: The measurement model is a mathematical expression, which expresses each measurement as a function of state variables. The state variables are defined as the minimum set of variables whose knowledge completely defines any other quantity in the instrumentation channel. The model of the instrumentation channel is shown in Figure 2. The state of the instrumentation channel is:

$$\mathrm{x}(t)=[v_1(t)\ v_2(t)\ v_3(t)\ v_4(t)\ e(t)\ \lambda(t)\ i_p(t)\ i_m(t)\ i_{L1}(t)\ i_{L2}(t)\ i_{L3}(t)\ ]$$

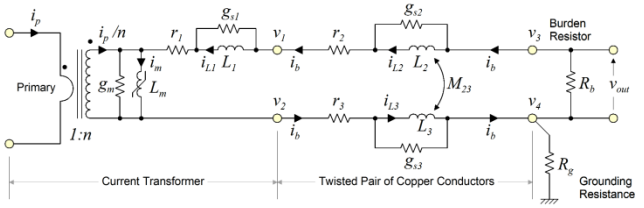

Figure 2: Equivalent circuit of current instrumentation channel

In a current instrumentation channel one measurement is taken, the current through the burden or the voltage across the burden. In addition, by considering the physical laws that the instrumentation channel must obey, we identify a number of virtual and derived measurements. Finally the ground point voltage is unknown (and difficult to measure). Since the voltage at the ground point is expected to be near zero, we introduce a pseudo-measurement for this point. The actual, virtual, derived and pseudo measurements are provided next.

Actual Measurements (1):

$$v_{out}(t)=v_3(t)-v_4(t)$$

Virtual Measurements (10)

KCL at node 0 yields:

$$0=-g_m e(t)-i_m(t)+\frac{1}{n}i_p(t)+\mathrm{i}_{L_1}(t)+g_{s1}L_1\frac{di_{L_1}(t)}{dt}$$

KCL at node 1 yields:

$$0=g_m e(t)+i_m(t)-\frac{1}{n}i_p(t)-\mathrm{i}_{L_2}(t)-g_{s2}\left(L_2\frac{di_{L_2}(t)}{dt}-M_{23}\frac{di_{L_3}(t)}{dt}\right)$$

KCL at node 2 yields:

$$0=-g_m e(t)-i_m(t)+\frac{1}{n}i_p(t)+\mathrm{i}_{L_3}(t)+g_{s3}\left(L_3\frac{di_{L_3}(t)}{dt}-M_{23}\frac{di_{L_2}(t)}{dt}\right)$$

KVL loop: node 1 to transformer to node 2, yields:

$$0=-v_1(t)+v_2(t)+e(t)+L_1\frac{di_{L_1}(t)}{dt}+r_1\left(g_m e(t)+i_m(t)-\frac{1}{n}i_p(t)\right)$$

KVL loop: node 3 to node 1, yields:

$$0=-v_3(t)+v_1(t)+r_2\left(\mathrm{i}_{L_2}(t)+g_{s2}\left(L_2\frac{di_{L_2}(t)}{dt}-M_{23}\frac{di_{L_3}(t)}{dt}\right)\right)+L_2\frac{di_{L_2}(t)}{dt}-M_{23}\frac{di_{L_3}(t)}{dt}$$

KVL loop: node 2 to node 4, yields:

$$0=-v_2(t)+v_4(t)+r_3\left(\mathrm{i}_{L_3}(t)+g_{s3}\left(L_3\frac{di_{L_3}(t)}{dt}-M_{23}\frac{di_{L_2}(t)}{dt}\right)\right)+L_3\frac{di_{L_3}(t)}{dt}-M_{23}\frac{di_{L_2}(t)}{dt}$$

KCL at node 3 yields:

$$0 = \mathrm{i}_{L_2}(t) + g_{s2}\left(L_2\frac{di_{L_2}(t)}{dt} - M_{23}\frac{di_{L_3}(t)}{dt}\right) + g_b\left(v_3(t) - v_4(t)\right)$$

KCL at node 4 yields:

$$0 = -\mathrm{i}_{L_3}(t) - g_{s3}\left(L_3\frac{di_{L_3}(t)}{dt} - M_{23}\frac{di_{L_2}(t)}{dt}\right) + g_b\left(v_4(t) - v_3(t)\right)$$

Transformer magnetizing leg yields:

$$0 = e(t) - \frac{d\lambda(t)}{dt}$$

$$0 = i_m(t) - i_0\left|\frac{\lambda(t)}{\lambda_0}\right|^n sign(\lambda(t)) - \frac{1}{L_0}\lambda(t)$$

Use as an example n=11. In this case (odd n) the above simplifies to:

$$0 = i_m(t) - i_0\left(\frac{\lambda(t)}{\lambda_0}\right)^n - \frac{1}{L_0}\lambda(t)$$

Derived Measurements (5):

$$i_b^m(t) = -g_b\left(v_3(t) - v_4(t)\right)$$

$$i_b^m(t) = \mathrm{i}_{L_1}(t) + g_{s1}L_1\frac{di_{L_1}(t)}{dt}$$

$$i_b^m(t) = \mathrm{i}_{L_2}(t) + g_{s2}\left(L_2\frac{di_{L_2}(t)}{dt} - M_{23}\frac{di_{L_3}(t)}{dt}\right)$$

$$i_b^m(t) = -\mathrm{i}_{L_3}(t) - g_{s3}\left(L_3\frac{di_{L_3}(t)}{dt} - M_{23}\frac{di_{L_2}(t)}{dt}\right)$$

$$i_b^m(t) = g_m e(t) + \mathrm{i}_m(t) - \frac{1}{n}i_p(t)$$

Pseudo Measurement, node 4 is grounded (1):

$$0^m = v_4(t)$$

There are 1+10+5+1=17 measurements. The number of states is 11.

Observe that one equation is nonlinear (exponent of 11). This equation is quadratized to yield the following quadratized measurement models. Additional variables $y_1\ y_2\ y_3\ y_4$ are introduced to decrease the order of each equation to 2.

$$0 = y_1(t) - \left(\frac{\lambda(t)}{\lambda_0}\right)^2$$

$$0 = y_2(t) - \left(y_1(t)\right)^2$$

$$0 = y_3(t) - \left(y_2(t)\right)^2$$

$$0 = y_4(t) - y_3(t)\cdot y_1(t)$$

$$0 = i_m(t) - i_0\left(\frac{\lambda(t)}{\lambda_0}\right)y_4(t) - \frac{1}{L_0}\lambda(t)$$

Now there are 1+14+5+1=21 measurements in the quadratized model. The number of states is 15. The state vector is

$$\mathrm{x}(t) = [v_1(t)\ v_2(t)\ v_3(t)\ v_4(t)\ e(t)\ \lambda(t)\ y_1(t)\ y_2(t)\ y_3(t)\ y_4(t)$$
$$i_p(t)\ i_m(t)\ i_{L1}(t)\ i_{L2}(t)\ i_{L3}(t)]$$

Note that there is a redundancy of measurements over the state vector of 6.

Subsequently the dynamic state estimation is applied using the above measurement model. The dynamic state estimation is an optimization problem which minimizes the differences between measurements and the values of the measurements obtained from the model. The solution of the optimization problem provides the best estimate of the state vector from the measurements. The dynamic state estimation is provided in the next section.

The measurements are stacked together and are written in a common syntax, which is referred to as dynamic quadratized measurement model. The presented quadratized measurement dynamic models are shown in the following matrix notation:

$$\mathbf{z(t)} = \mathbf{h}(\mathbf{x}(t)) = \mathbf{Y_{m,x}}\mathbf{x}(t) + \mathbf{D_{m,x}}\frac{d\mathbf{x}(t)}{dt} + \left\{\begin{array}{c}\vdots\\ \mathbf{x}(t)^T\left\langle F_{m,x}^i\right\rangle\mathbf{x}(t)\\ \vdots\end{array}\right\} + \mathbf{C_m} + \boldsymbol{\eta}$$

Where: $\mathbf{z(}t\mathbf{)}$ is the measurement vector (actual, derived, pseudo and virtual measurements), $\mathbf{x}(t)$ is the state variable vector, $\mathbf{Y_{m,x}}$ is the matrix defining the linear part for state variables, $\mathbf{D_{m,x}}$ is matrix defining the differential part for state variables, $\mathbf{C_m}$ is the constant vector of the measurement model, $\mathbf{F_{m,x}}$ is the matrix defining the quadratic terms, and $\boldsymbol{\eta}$ is the error vector.

*A. **Dynamic AQCF Measurement Model**:* Quadratic integration method is used to convert the dynamic measurement model to algebraic form, which is referred as Algebraic Quadratic Companion Form (AQCF) measurement model [14]. The quadratic integration is based on a numerical integration method that assumes that time domain functions vary quadratically within an integration time step. The integration links the values of the state and measurements at time stamp t, t-h, and t_m (intermediate time stamp of t and $t-h$). The quadratic integration method is an implicit numerical integration and therefore demonstrates the desired advanced numerical stability properties compared to explicit methods [15]. The resultant mathematical model of the measurements is:

$$\mathbf{z}(t,t_m) = \mathbf{h}(\mathbf{x}(t,t_m)) = \mathbf{Y_z}\mathbf{x}(t,t_m) + \left\{\begin{array}{c}\vdots\\ \mathbf{x}(t,t_m)^T F_z^i\mathbf{x}(t,t_m)\\ \vdots\end{array}\right\} + \mathbf{N_z}\mathbf{x}(t-h) + \mathbf{M_z}i(t-h) + \mathbf{K_z} + \boldsymbol{\eta_z}$$

where $\mathbf{z}(t,t_m)$ is the measurement at two adjacent time instances time t and time t_m. $\mathbf{Y_z}$ is linear term coefficient matrix, $\mathbf{F_z}$ is quadratic term coefficient matrix, $\mathbf{N_z}$ is past history linear term coefficient matrix, $\mathbf{M_z}$ is past history current term coefficient matrix, $\mathbf{K_z}$ is past history constant vectors and $\boldsymbol{\eta_z}$ is error vectors. Note that the sample values are taken at 80 samples per cycle, the integration time step h is two sampling periods, i.e. 416.666 microseconds.

Dynamic State Estimation Method

The dynamic state estimation provides the best estimate of the states from the measurements, in this case redundant measurements. Considering the measurement model provided earlier, it is clear that each measurement, at time t or time t_m is given as a function of the state and some unknown measurement error (note the state at time t-h is assumed known from past computations), i.e.

$$z_i(t,t_m) = h_i\left(x(t,t_m)\right) + \eta_i, \quad i = 1, 2, 3, ..., m$$

Where: m is the total number of measurements, z_i is the measurement i, $h_i(x)$ is the equation expressing the measurement i as a function of the state x, and η_i is the measurement error with the following statistics:

$$E[\eta_i] = 0, \quad Var[\eta_i] = \sigma_i^2, \quad E[\eta_i \eta_j] = 0$$

Where σ_i is the standard deviation of the corresponding measurement z_i. The value of σ_i for actual, derived, virtual, and pseudo measurement is 0.05% p.u., 0.05% p.u., 0.005% p.u. and 10% p.u., respectively.

The state estimation problem can be solved with the WLS (Weighted Least Squares) method which is defined with:

$$Min\ J = \left(\mathbf{z}(t,t_m) - \mathbf{h}\left(\mathbf{x}(t,t_m)\right)\right)^T \mathbf{W}\left(\mathbf{z}(t,t_m) - \mathbf{h}\left(\mathbf{x}(t,t_m)\right)\right)$$

Where the weight matrix $\mathbf{W} = diag(\cdots, \frac{1}{\sigma_i^2}, \cdots)$.

The best estimate of the state is obtained from the Gauss-Newton iterative algorithm:

$$\hat{\mathbf{x}}(t,t_m)^{\nu+1} = \hat{\mathbf{x}}(t,t_m)^{\nu} + (\mathbf{H}^T\mathbf{W}\mathbf{H})^{-1}\mathbf{H}^T\mathbf{W}(\mathbf{z}(t,t_m) - \mathbf{h}(\hat{x}(t,t_m)^{\nu}))$$

where $\hat{\mathbf{x}}(t,t_m)$ refers to the best estimate of the state vector $\mathbf{x}(t,t_m)$, and $\mathbf{H} = \partial\mathbf{h}(\mathbf{x}(t,t_m)) / \partial\mathbf{x}(t,t_m)$ is the Jacobean matrix of the measurement equations.

The normalized residuals $\mathbf{r}(t,t_m) = \sqrt{\mathbf{W}}(\mathbf{z}(t,t_m) - \mathbf{h}(\hat{\mathbf{x}}(t,t_m))$ are computed at the solution $\hat{\mathbf{x}}(t,t_m)$. Subsequently, the confidence level $P_{conf}(t)$, which expresses the probability of goodness of fit between measurements and dynamic model within meter accuracy, is computed from the normalized residuals:

$$\zeta(t) = \mathbf{r}(t,t_m)^T\, \mathbf{r}(t,t_m)$$

$$P_{conf}(t) = \Pr\left[\chi^2 \geq \zeta(t)\right] = 1 - \mathrm{P}(\zeta(t), v)$$

where $\mathrm{P}(\zeta(t), v)$) is the probability of $\chi 2$ distribution given $\chi^2 \leq \zeta(t)$ with degrees of freedom $v = m - n$.

Importance of Intrumentation Channel Math Model

The presented method requires a high fidelity model of the instrumentation channel including the CT model. Models for the cables, merging unit burden and A/D conversion are well known. Deriving a high fidelity model of the CT is typically challenging but it is doable. We developed a method to derive the model of the CT from manufacturer data as well as manufacturer test data. The method has been tested in the laboratory and the results are quite accurate between the model and test results. The method with performance analysis is shown in Appendix A. Note that the CT model utilized in the previous section is the one presented in Appendix A. The model is accurate for low frequencies, typically, zero to 1000 Hz.

Example Results

An example test system is utilized to model instrumentation channels and merging units to create simulated data of primary currents and measured values at the merging units. Subsequently, the measured values at the merging unit are used in the dynamic state estimation to provide the best estimate of primary current. Since the primary current is known form the simulation, the absolute error of the method can be computed, thus providing and excellent measure of performance of the proposed method.

The example test system is presented in Figure 3. It comprises a 115-kV transmission system. A current transformer measures phase A current of the line that is located on the left hand side of the figure. The CT ratio is 800:5A, and the error class for the CT is 10C100. The instrumentation cable is #10 cable with the length 96 meters. The burden resistance is 0.1 Ω.

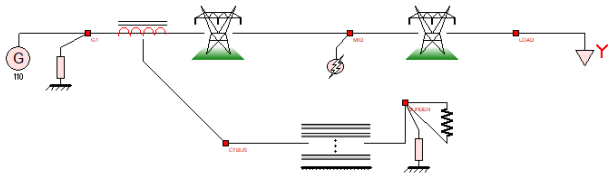

Fig. 3 Example system for current instrumentation channel error correction

Event 1: Low CT saturation: A phase A to ground fault at bus MID (middle of figure 3) was simulated. This fault yields fault current that causes low CT saturation of the instrumentation channel. The merging unit measures the CT secondary current through the burden resistor, as shown in

Figure 4. It can be seen in Figure 4 that the CT secondary current is moderately distorted.

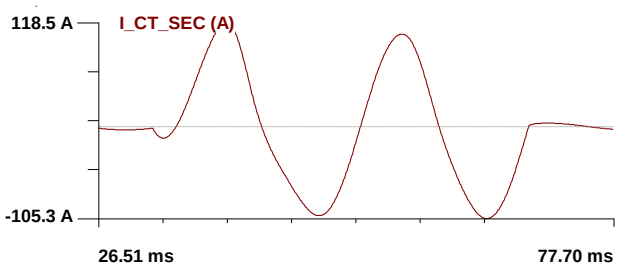

Figure 4: CT secondary current through the burden resistor

Application of the current instrumentation channel error correction algorithm provides the best estimate of the CT primary current. Figure 5, top set of traces, provides a graph of the estimated primary current, the actual primary current and the primary current computed by simply multiplying the measurement secondary current time the transformation ratio. The last quantity is referred to as "Ratio*CT Secondary Current". Note a sizable difference between the last quantity and the actual primary current. On the other hand the estimated primary current tracks very well the actual primary current. The bottom set of traces of Figure 5 provides the error between the uncorrected primary current and the actual primary current as well as the error between the estimated and actual primary current. Note that without error correction the error reaches 50% while with error correction the error is below 1%.

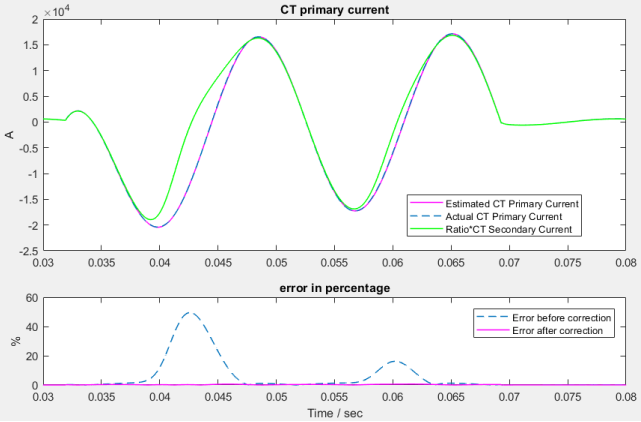

Figure 5: Comparison between the CT primary current before and after correction

Event 2: Deep CT Saturation: A phase A to phase C fault at bus MID (middle of figure 3) was simulated. This fault yields fault current that causes high CT saturation of the instrumentation channel. The merging unit measures the CT secondary current through the burden resistor, as shown in Figure 6. It can be seen in Figure 6 that the CT secondary current is highly distorted.

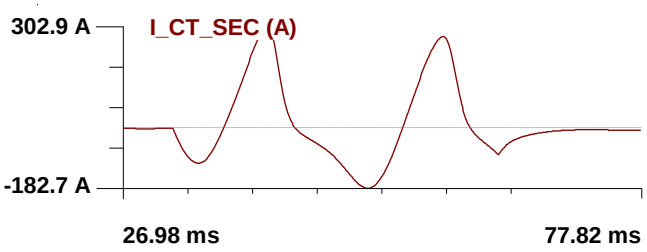

Figure 6: CT secondary current through the burden resistor

Application of the current instrumentation channel error correction algorithm provides the best estimate of the CT primary current. Figure 7, top set of traces, provides a graph of the estimated primary current, the actual primary current and the primary current computed by simply multiplying the measurement secondary current time the transformation ratio. The last quantity is referred to as "Ratio*CT Secondary Current". Note a large difference between the last quantity and the actual primary current. On the other hand the estimated primary current tracks very well the actual primary current. The bottom set of traces of Figure 5 provides the error between the uncorrected primary current and the actual primary current as well as the error between the estimated and actual primary current. Note that without error correction the error exceeds 200% while with error correction the error is below 2.5%.

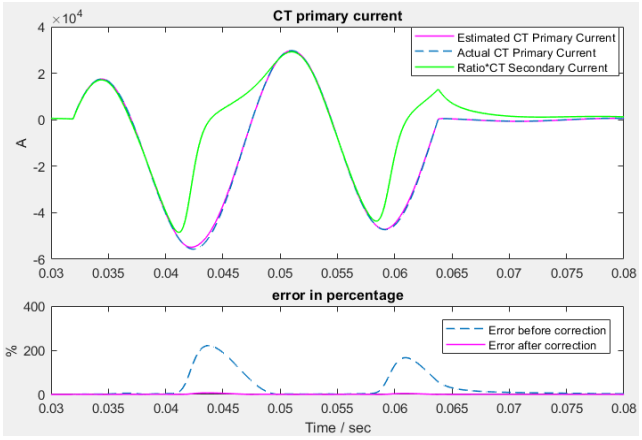

Figure 7: Comparison between the CT primary current before and after correction

CONCLUSIONS

This paper proposes an on-line current instrumentation channel error correction method using dynamic state estimation. The method can be integrated with the merging units so that they directly provide corrected values of the primary quantities. The method has been demonstrated on current instrumentation channels. It can reliably reproduce the primary current under various saturation conditions of the CT. The computation of the method can be performed within a fraction of one sampling interval of merging units. This

additional latency does not cause any problems in the streaming of the data from the merging units. The method can be applied equally well on voltage instrumentation channels.

REFERENCES

[1] [1] Jiuping Pan, Khoi Vu and Yi Hu, "An efficient compensation algorithm for current transformer saturation effects," *IEEE Trans. Power Delivery*, vol. 19, no. 4, pp. 1623-1628, Oct. 2004.

[2] [2] Y. C. Kang, J. K. Park, S. H. Kang, A. T. Johns and R. K. Aggarwal, "An algorithm for compensating secondary currents of current transformers," *IEEE Trans. Power Delivery*, vol. 12, no. 1, pp. 116-124, Jan 1997

[3] Yong Cheol Kang, Ui Jai Lim, Sang Hee Kang and P. A. Crossley, "Compensation of the distortion in the secondary current caused by saturation and remanence in a CT," *IEEE Trans. Power Delivery*, vol. 19, no. 4, pp. 1642-1649, Oct. 2004.

[4] Z. Lu, J. S. Smith and Q. H. Wu, "Morphological Lifting Scheme for Current Transformer Saturation Detection and Compensation," *IEEE Trans. Circuits and Systems I*: vol. 55, no. 10, pp. 3349-3357, Nov. 2008.

[5] D. C. Yu, J. C. Cummins, Z. Wang, Hong-Jun Yoon, L. A. Kojovic and D. Stone, "Neural network for current transformer saturation correction," *1999 IEEE Transmission and Distribution Conf.*, New Orleans, LA, 1999, pp. 441-446 vol.1

[6] D. C. Yu, J. C. Cummins, Zhudin Wang, Hong-Jun Yoon and L. A. Kojovic, "Correction of current transformer distorted secondary currents due to saturation using artificial neural networks," *IEEE Trans. on Power Delivery*, vol. 16, no. 2, pp. 189-194, Apr 2001.

[7] H. Khorashadi-Zadeh and M. Sanaye-Pasand, "Correction of saturated current transformers secondary current using ANNs," *IEEE Trans. Power Delivery*, vol. 21, no. 1, pp. 73-79, Jan. 2006.

[8] Y.-Y Hong and P.-C Chang-Chian, "Detection and correction of distorted current transformer current using wavelet transform and artificial intelligence", *IET Generation, Transmission & Distribution*, vol. 2, no. 4, pp. 566-575, July 2008

[9] Jiuping Pan, Khoi Vu and Yi Hu, "An efficient compensation algorithm for current transformer saturation effects," *IEEE Trans. Power Delivery*, vol. 19, no. 4, pp. 1623-1628, Oct. 2004.

[10] C. S. Yu, "Detection and Correction of Saturated Current Transformer Measurements Using Decaying DC Components," *IEEE Trans. Power Delivery*, vol. 25, no. 3, pp. 1340-1347, July 2010.

[11] Y. C. Kang, S. H. Ok, S. H. Kang and P. A. Crossley, "Design and evaluation of an algorithm for detecting current transformer saturation," in IEE Proceedings - Generation, Transmission and Distribution, vol. 151, no. 1, pp. 27-35, 14 Jan. 2004.

[12] H. Dashti, M. Sanaye-Pasand and M. Davarpanah, "Fast and Reliable CT Saturation Detection Using a Combined Method," in IEEE Transactions on Power Delivery, vol. 24, no. 3, pp. 1037-1044, July 2009.

[13] Takoi K. Hamrita, Bonnie S. Heck, and A.P.Sakis Meliopoulos, "On-line correction of errors introduced by instrument transformers in transmission-level steady-state waveform measurements," *IEEE Trans. Power Delivery*, vol. 15, no. 4, pp. 1116-1120, Oct 2000.

[14] A. P. S. Meliopoulos et al., "Dynamic State Estimation-Based Protection: Status and Promise," in IEEE Transactions on Power Delivery, vol. 32, no. 1, pp. 320-330, Feb. 2017.

[15] G. K. Stefopoulos, G. J. Cokkinides and A. P. Meliopoulos, "Quadratic integration method for transient simulation and harmonic analysis," *2008 13th International Conf. on Harmonics and Quality of Power*, Wollongong, NSW, 2008, pp. 1-8

APPENDIX A: CURRENT TRANFORMER MODEL CONSTRUCTION

The parameters of a CT non-linear dynamic model can be obtained by measuring the RMS current at the CT secondary winding for various voltages applied across the CT secondary. The test circuit is illustrated in Figure A-1. In order to evaluate the measurement procedure, a 200:5 low accuracy CT was characterized using this setup. The voltage across the CT secondary was varied from 50 mV to 10 Volts RMS. The measured secondary RMS current versus secondary RMS voltage were directly obtained using the oscilloscope waveform analysis functions. The applied voltage range was selected so that both linear and saturation regions of the CT are captured. The measured data were plotted on logarithmic scale making sure that the decade lengths on the vertical and horizontal axis are equal. Then a 45-degree tangent line was drawn identifying the saturation point at 3 Volts and 173 mA RMS, see Figure A-2. Next, an impedance bridge was used to measure the secondary DC Resistance. The result was 41 milli-Ohms. The test data were used to set the WinIGS model parameters. Specifically, the slope of the VI curve in the saturation region was used to set the model saturation equation exponent (n). Then, the magnetizing current and core conductance model parameters were adjusted so that the calculated VI curve closely matches the curve obtained from measurements. The final selected parameters and computed VI curve, are illustrated in Figure A-3.

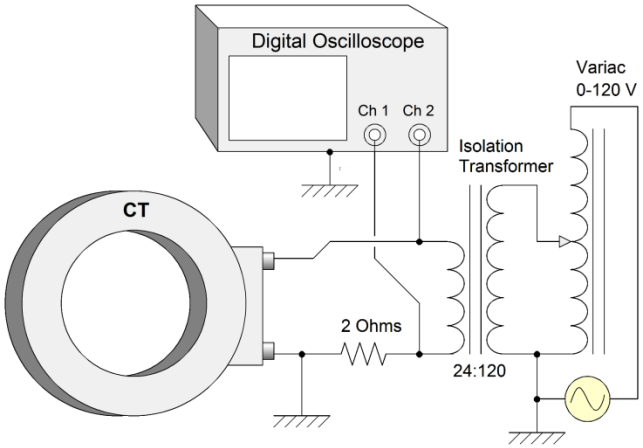

Figure A-1: CT Saturation Test Circuit

Next, the same CT was tested and simulated under sever saturation in order to evaluate the model accuracy. The test setup is illustrated in Figure A-4. The CT primary current was 198 A at 60 Hz (peak value 280 A), with a 2 Ohm Burden connected at the secondary (the values were so selected as to drive the CT into saturation). Under these conditions, the secondary current was measured at 3.37 Amperes. Note that this value is 28% lower than value obtained by multiplying the primary current by the nominal CT ratio (198 x 5 / 200 = 4.95 A). The simulation results are illustrated in Figure A-5. The test results are shown in Figure A-4. Note that the simulated secondary current (burden current trace) is 3.57 Amperes. These measurements were compared to the values provided by the model and the match is excellent.

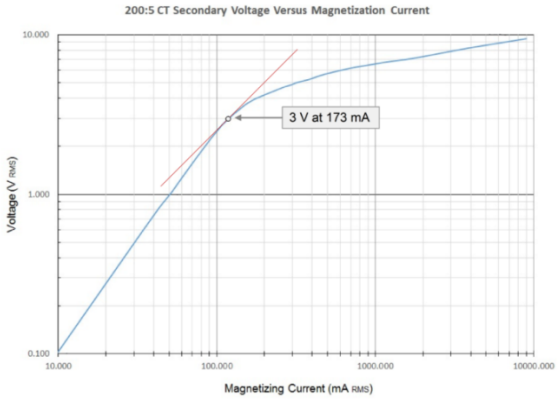

Figure A-2: CT Saturation Curve as determined by Test

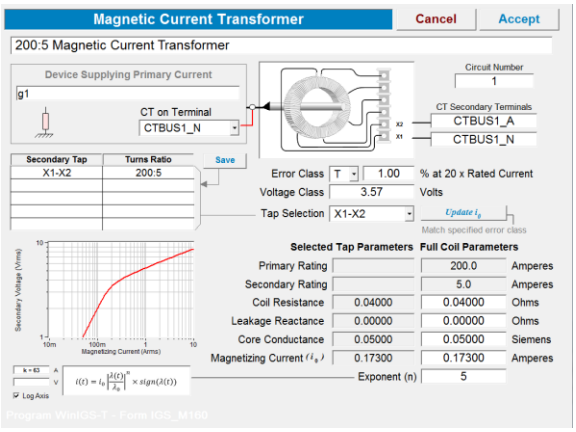

Figure A-3: CT Model Parameters

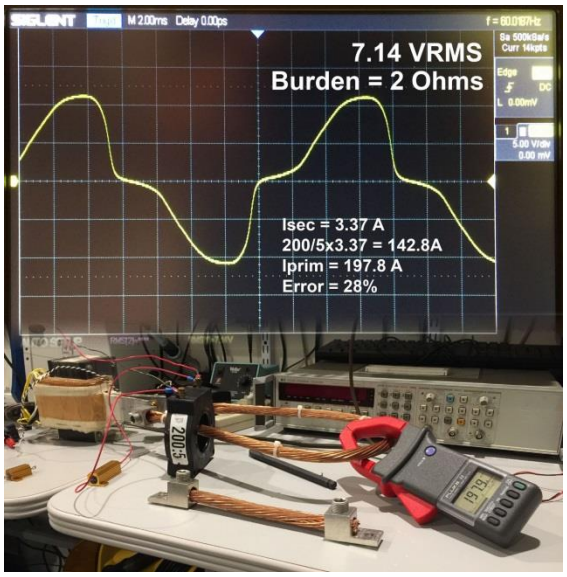

Figure A-4: Measured CT Secondary Voltage Waveform

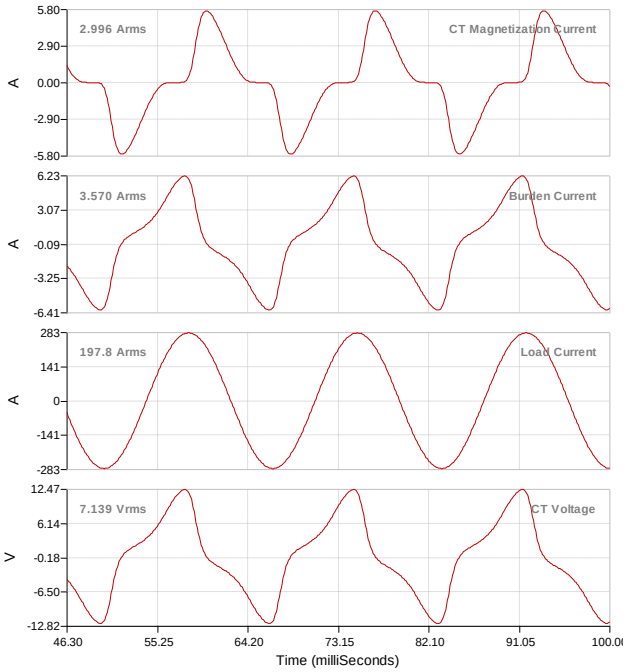

Figure A-5: Measured CT Secondary Voltage Waveform